Scanning Microdeformation Microscopy: Advances in quantitative micro and nanometrology.

Authors: P. Vairac, J. Le Rouzic, P. Delobelle, B. Cretin

FEMTO-ST Institute, Université de Franche-comté, CNRS, ENSMM, UTBM
32 avenue de l'Observatoire - 25044 Besançon Cedex – France

Correspondence:

P. Vairac, FEMTO-ST Institute, 32 avenue de l'Observatoire, 25044 Besançon Cedex - France
e-mail : pascal.vairac@femto-st.fr ;
tel. +33 3 81 85 39 99 ;
fax. +33 3 81 85 39 98

Abstract:
The SMM is a well known scanning acoustic probe technique. Recently in the last years in order to optimize this metrological instrument a sensitivity study was carried out to adapt the stiffness of the microcantilevers to the encountered contact stiffnesses. The accuracy of the measurement is so optimized for the elasticity of the sample to characterize. Problems coming from the sliding of the tip on the surface and their effects were exhibited. New specific geometries of microcantilevers were conceived to reduce these perturbations. Their use reduced significantly the slip and so led to a better determination of the resonance frequencies, even for high amplitudes of vibration.
In a last part a study of mechanical characterization was realized on polymers using DMA, SMM and nanoindentation. The use of different techniques enables to obtain complementary measures (viscoelastic characterization for several decades).

- Introduction

Knowledge of the mechanical properties of materials at local scale has become a major issue in engineering because of the miniaturization of devices. The development of Microelectromechanical Systems (MEMS) has been thanks to the deposition techniques of thin films (submicron thickness). Most of the time, MEMS are composed of multiple layers of different materials. However, the mechanical properties of such surfaces are difficult to predict. They can vary considerably depending on the techniques clean room use. Moreover, at such scales, it is difficult to use the laws of continuum mechanics to predict the mechanical behavior of these thin films. It is therefore vital to have reliable measurement techniques to meet these needs.

During the last twenty years, near-field microscopes have been developed in order to increase the lateral resolution and to measure different local properties of the investigated material. Main achieved systems have been derived from the AFM. The combination between AFM and acoustics, often designed AFAM emerged after 1992[1-6]. Many features have been discovered and have been investigated from both theoretical to experimental domains. All these near-field microscopes have a behavior based on the concept of FMM (Force Modulation Microscopy).

The force modulation microscope was first introduced by Maivald and al [7]. A periodic displacement at low frequency (few kHz) is imposed on the sample using a piezoelectric ceramic. The tip in contact with the sample follows the harmonic vibrations. Measuring the amplitude of the displacement of cantilever provides information on local variations of elasticity of the sample. Use of cantilevers with high stiffness leads to large applied forces and facilitates contacts plastic nature limiting the possibilities of quantitative measurements of the elasticity of the surface. A variant of this technique is to apply an external force at the end of the cantilever. This is called direct force modulation as opposed to the previous method which is called indirect force modulation. Practically this external force can be applied either locally with a magnet glued to the end of the lever subjected to a harmonic magnetic field created by a coil, or more broadly with a magnetic film deposited on the entire lever [8,9]. Compared to an indirect force modulation cantilever stiffness is low enough, which reduces the risk of plastic deformation.

The Scanning Microdeformation Microscope (SMM) is also a dynamic force microscope, but conversely to the most part of near-field microscopes based on the AFM, the sensor is magnified by one or two orders of magnitude[1,2,10]. The SMM can operate in transmission mode: a piezoelectric ceramic detects the acoustic amplitudes transmitted through the sample allowing subsurface imaging. The other way of detection is to measure the amplitude and the phase of the vibration of the cantilever with a high sensitive optical interferometer pointing onto the cantilever in elastic contact with the sample. The radius of the SMM sensor tip is larger than the radius of an AFM tip and for these reason models used to characterize the tip-sample interaction are easier to apply allowing “true” quantitative measurement of elastic properties of sample, even if the lateral resolution is lower than in AFM based techniques.

The aim of this chapter is to present the last advances in term of quantitative measurement at local scale particularly with the SMM, and how it can be complementary with other mechanical tools for local characterization.

The chapter in a first time describes the SMM and the physical basis of the behaviour and modeling. A specific study dedicated to optimization of the sensitivity SMM is detailed, showing that it is necessary to adapt the stiffness of the microcantilevers to the encountered contact stiffnesses. The accuracy of the measurement is so optimized for the elasticity of the sample to characterize. In some operating ranges of these near-field microscopes, the sliding effect of tip on the surface of the sample generates in many cases a problem of localization of the measurement and non linear perturbations. In order to reduce these effects, specific geometries of microcantilever have been studied. Their use reduced significantly the slip and so led to a better determination of the resonance frequencies, even for high amplitudes of vibration.

The last part of the chapter is devoted to a complete study of local properties of polymers by coupling the measurement results obtained with the SMM with two others techniques: nanoindentation and Dynamic Mechanical Analysis. The use of different techniques enables to obtain complementary measures on viscoelastic characterization for several decades.

1 - The Scanning Microdeformation Microscope

1.1 – The experimental set-up

The experimental set-up called SMM is shown in figure 1. As in AFM a 3-axis translation unit supports the sample. The vertical axis enables to adjust the value of the static contact force.

The head of the microscope is composed of a piezoelectric transducer, the cantilever and the tip (made of diamond or sapphire and not of silicon as in standard AFM where the tip is obtained by chemical etching of the cantilever). This hybrid sensor can be considered as an electromechanical resonator whose frequency is related to the tip-sample interaction. The tips can be standard pickup needles of sapphire (15 to 45 µm radii), or specific diamond tips with radius down to 0.6 µm. Depending on the tip radius and the applied force, the contact radius is in the 50 nm-2µm range.

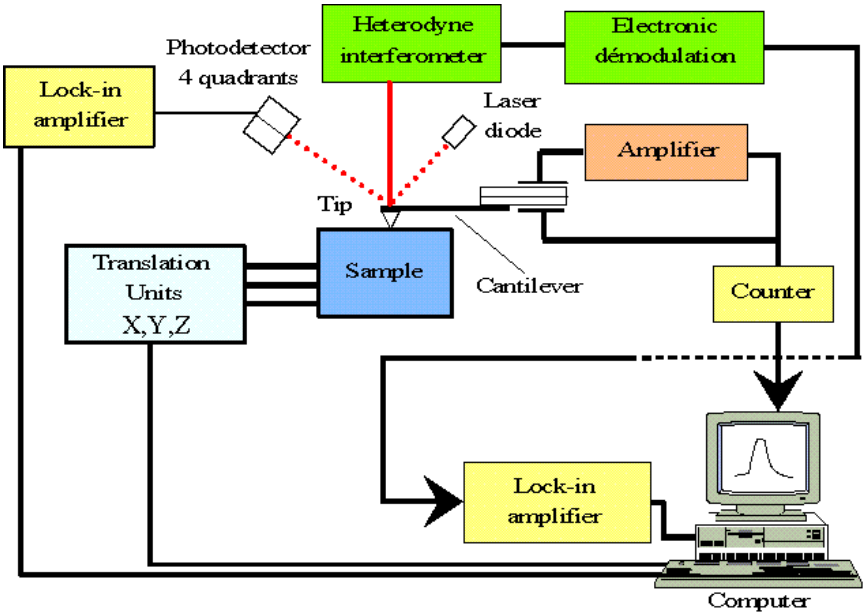

Figure 1: Experimental set-up of the SMM which allows to control the static force between the tip and the sample and to measure quantitatively the vibration of the sample surface with a high sensitivity.

The tip is kept in flexural vibration with the low frequency generator. The heterodyne interferometer is used as a non-invasive sensor to detect quantitatively the amplitude and the phase of the vibrating cantilever and the surface sample. The principle of this interferometer developed for out-of-plane vibrations measurement is completely described in refs [11-13]. After the electronic demodulation, a lock-in-amplifier allows to obtain a high sensitivity. In ideal conditions the ultimate sensitivity is about 1fm/√Hz.

Moreover we used on the SMM the classical optical beam deflection system modified to obtain a dynamic detection of the static deflection of the cantilever. More precisely we modulated the laser diode and we detected the amplitude and the phase of the static deflection with a lock-in-amplifier. By this way it is possible to evaluate the static force and the static indentation on the sample.

This microscope is an effective tool to image surfaces and subsurfaces with heterogeneous local elasticity or to characterize elastic properties of a material. Some examples of images presented below demonstrate these characteristics.

First presented sample is a silicon wafer (360 µm thickness, crystalline orientation [100]). Parallel grooves have been etched on one face, the opposite face remained polished. A cross section of the sample which was coupled to the support with an ultrasonic gel is showed figure 2a. Scanned surface is the plane face of the sample where the grooves are optically invisible. Figure 2b shows the frequency image obtained with a tip having a 40 µm radius.

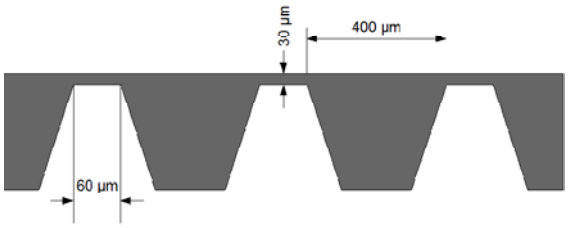

a)

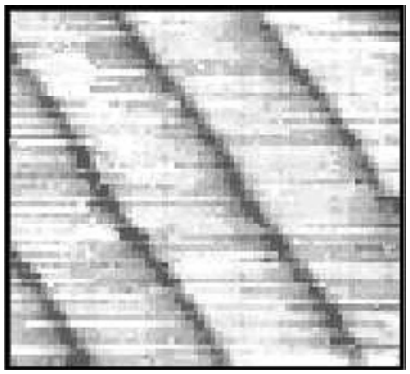

b)

Figure 2 a) Geometry of the etched silicon sample**. b)** Image of the subsurface grooves obtained at 18 kHz with a frequency variation of 100Hz (image size: 2000 x 2000 µm)[2].

Subsurface grooves appear as parallel black stripes (the harder the sample surface, the higher the frequency).

The second sample is made of duralumin (AU4G). A 50 µm diameter tungsten wire was inserted in a diffusion bond. The sample was cut and polished progressively, so that the tungsten wire just appeared on the sample side (figure 3a). In the image area the tungsten wire-surface spacing is estimated to be 25-35 µm. The frequency image in Figure 3b obtained at 17 kHz shows the detection capability of the SMM. Small scratches resulting from contact can be observed on the sample surface.

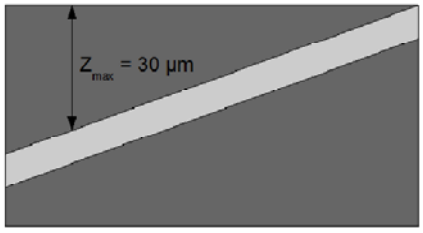

a)

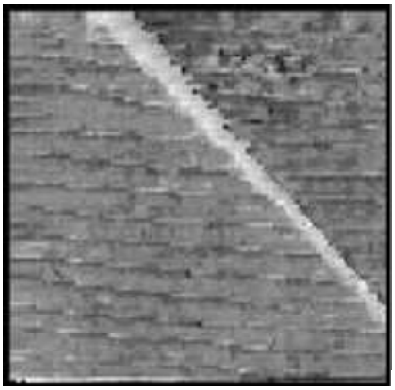

b)

Figure 3a) Cross section of the sample. **b)** Microdeformation image of the tungsten wire obtained at 17 kHz with a frequency variation of 500 Hz (image size: 500 x 500 μm)[2].

The present results demonstrate that the SMM can give images of subsurface defects with image contrast related to the properties of the microdeformation volume in the case of polished surfaces.

In a more quantitative method of operation we use the SMM to determine the local Young's modulus of material. So we put the tip in contact with the sample and we apply an additional static force by vertically displacing the clamped end of the cantilever. Then we scan the excitation frequency. The resonant frequency depends on the static force applied via the contact stiffness. Currently, measuring the resonant frequency, we can estimate the local contact stiffness and then with a suitable model, the local Young's modulus with high accuracy. Other ultrasonic noninvasive methods such as atomic force acoustic microscope, ultrasonic force microscopy, or AFM spectroscopy with heterodyne interferometer make such a characterization on the nanometer scale but with less accuracy, because the contact model must take into account additional forces on this scale.[14-17]. We can also notice the nanoindentation and particularly Continuous Stiffness Measurement technique which is a destructive method which enables local elasticity measurements.[18]

1.2 – The basic model

We have used a continuous model[19,20] (Fig. 4) to describe the physical behavior of the SMM, and to obtain Young's moduli values of tested samples from the measured contact resonant frequencies. The cantilever is represented as a beam interacting with the sample through two springs k^* and k_{lat}. The piezoelectric bimorph transducer action on the cantilever has been modeled as simple mass m_p and spring k_p.

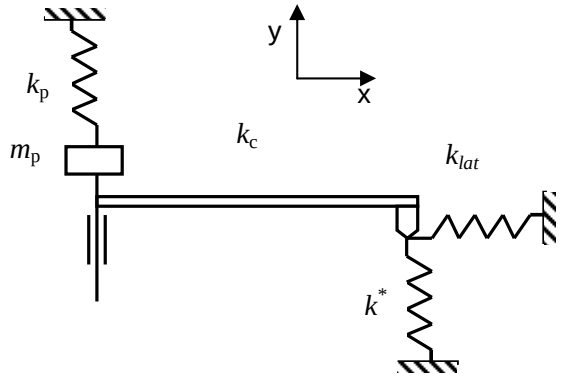

Figure 4: Model used to describe the behavior of the SMM.

The longitudinal interaction stiffness k* and the lateral interaction stiffness klat have to be known in order to evaluate the stiffness of the sample. On a mesoscopic scale and in the ideal case of flat sample, k* can be estimated by using the classical contact theory of Hertz when the tip (assumed to be a spherical indenter of radius R) contacts the sample [21]:

$$k^* = (6RE^{*2}F_0)^{1/3} = 2E^* a \qquad (1)$$

Where a is the contact radius, and E* the effective Young's modulus of the tip-sample contact.
As previously described, a sinusoidal vibration of the cantilever base is used as excitation, but a variable displacement offset of the sample Δz is also introduced to provide a static force. Thus this static force applied on the sample is related to Δz and to the longitudinal stiffness by the following expression:

$$F_0 = \frac{k_c k_{iL}}{k_c + k_{iL}} \Delta z \approx k_c \Delta z \qquad (2)$$

(This approximate relation can be applied for $k^* >> k_c$ where k_c is the stiffness of the cantilever).
With:

$$\frac{1}{E^*} = \frac{1-\nu_t^2}{E_t} + \frac{1-\nu_s^2}{E_s} = \frac{1-\nu_s^2}{E_s} \qquad (3)$$

Where E_t, ν_t and E_s, ν_s are, respectively, Young's modulus and Poisson ratio of the tip and the sample.
Mindlin theory on the contact between a sphere and a plane[21] makes possible to take into account the lateral stiffness and gives the relation between the longitudinal and lateral stiffness,

$$k_{lat}^* = 4k^* \frac{G^*}{E^*} \qquad (4)$$

With G* the reduced shear modulus expressed as:

$$G^* = \left(\frac{2(1+\nu_t)(2-\nu_t)}{E_t} + \frac{2(1+\nu_s)(2-\nu_s)}{E_s} \right)^{-1} \quad (5)$$

And finally:

$$k_{lat} \approx \frac{2(1-\nu_s)}{(2-\nu_s)} k^* \quad (6)$$

The most classical way to study this mechanical model is to solve the fourth-order differential equation for flexural vibrations of the cantilever[19,20] with the different applied boundary conditions:

$$EI \frac{\partial^4 y}{\partial x^4} + \rho A \frac{\partial^2 y}{\partial t^2} = 0 \quad (7)$$

where E is Young's modulus, I the area moment of inertia, ρ the volume density, and A the cross section of the cantilever. This equation describes the propagation of the dispersive flexural waves with the following relation:

$$EI\mu_n^4 - \rho A \omega_n^4 = 0 \quad (8)$$

ω_n being the angular frequencies and μ_n the associated eigenvalues.

Assuming a general solution of the following type for eq. 7:

$$\begin{aligned} y(x,t) &= \left[C_1\left(A^+\right) + C_2\left(A^-\right) + C_3\left(B^+\right) + C_4\left(B^-\right) \right] e^{j\omega t} \\ &= y(x) e^{j\omega t} \end{aligned} \quad (9)$$

where: $A^+_- = \cos(\mu x)^+_- \cosh(\mu x)$ and $B^+_- = \sin(\mu x)^+_- \sinh(\mu x)$

The constants C1-4 are determined by the boundary conditions applied to the cantilever.
At the excitation end of the cantilever (x=0) the boundary conditions are:

$$\begin{cases} \dfrac{\partial y(x)}{\partial x} = 0 \\ \dfrac{\partial^3 y(x)}{\partial x^3} = \dfrac{k_p}{EI} y(x) + \dfrac{m_p}{EI} \dfrac{\partial^2 y(x)}{\partial t^2} \end{cases} \quad (10)$$

At the interaction end (x=L), we can express the boundary conditions as:

$$\begin{cases} \dfrac{\partial^2 y(x)}{\partial x^2} = -l\dfrac{k_{il}}{EI}(x) + \dfrac{m}{EI}\dfrac{l_c^2}{l}\dfrac{\partial^2(x)}{\partial t^2} \\ \dfrac{\partial^3 y(x)}{\partial x^3} = \dfrac{k_{iL}}{EI}y(x) + \dfrac{m}{EI}\dfrac{\partial^2 y(x)}{\partial t^2} \end{cases} \quad (11)$$

Assuming that the displacement of the centre of the mass m in the x direction is smaller than that of the tip extremity by a factor lc/l (lc is the distance between the centre mass of the tip and the cantilever and l the length of the tip).

The general solution (eq. 9) and its derivatives are reported in these four boundary conditions and we obtain these relations between the constants $C_{1\text{-}4}$:

$C_3=0$

$C_4=\theta C_1$ with $\theta = -\dfrac{k_p}{\mu^3 EI} + \dfrac{m_p\omega^2}{\mu^3 EI}$

$$\frac{C_1}{C_2} = \frac{\beta(\cos\mu L + \cosh\mu L) - (\sin\mu L + \sinh\mu L)}{\beta[(-\cos\mu L + \cosh\mu L) - \theta(\sin\mu L + \sinh\mu L)] - [(-\sin\mu L + \sinh\mu L) + \theta(\cos\mu L - \cosh\mu L)]} \quad (12)$$

$$\frac{C_1}{C_2} = \frac{(\cos\mu L - \cosh\mu L) - \alpha(\sin\mu L - \sinh\mu L)}{\alpha[-\theta(\cos\mu L + \cosh\mu L) + (\sin\mu L + \sinh\mu L)] - [\theta(\sin\mu L - \sinh\mu L) + (\cos\mu L + \cosh\mu L)]} \quad (13)$$

with $\alpha = \dfrac{\mu^3}{\frac{k_{iL}}{EI} - \frac{m\omega^2}{EI}}$ and $\beta = \dfrac{\mu}{-\frac{k_{il}l^2}{EI} - \frac{ml_c^2\omega^2}{EI}}$

Finally the characteristic equation of the system is obtained by:

(12)=(13) (14)

and the solutions $\mu_n L$ of (14) computed with the software Maple, allow us to compute the resonance frequencies ω_n by using eq. 8.

The solution y(x,t) can be expressed in the form:

$$y(x,t) = y_0\left[(\cos\mu x + \cosh\mu x) + \frac{C_2}{C_1}(\cos\mu x - \cosh\mu x) + \theta(\sin\mu x - \sinh\mu x)\right]e^{j\omega t} \quad (15)$$

Depending on the parameters that we seek to determine, we will resolve the direct or the inverse problem.

- Direct problem:

Knowing the Young's modulus of the sample, we can evaluate, with the Hertz contact, the contact stiffness corresponding to some static force. Then from the stiffness of contact, we determine the eigenvalues μ_n. We obtain the frequencies of vibration modes and their associated deformation shape.

- Inverse problem:

We measure experimentally the resonant frequency of the cantilever that is injected into the model. We deduce the eigenvalue associated μ_n. With the model, we can then estimate the contact stiffness k*. Hertz's theory provides us a final measurement of Young's modulus of the sample.

Figure 5 shows the calculation performed on a silicon surface (100) with a static force of 0.8 mN. We experimentally measure a frequency of 28050 Hz for the first mode, which corresponds to an eigenvalue $\mu_1 L = 4.607$. We therefore find a contact stiffness of 163036 $N.m^{-1}$. Finally, taking 0.28 for Poisson's ratio, we calculate a Young's modulus of 129.1 GPa.

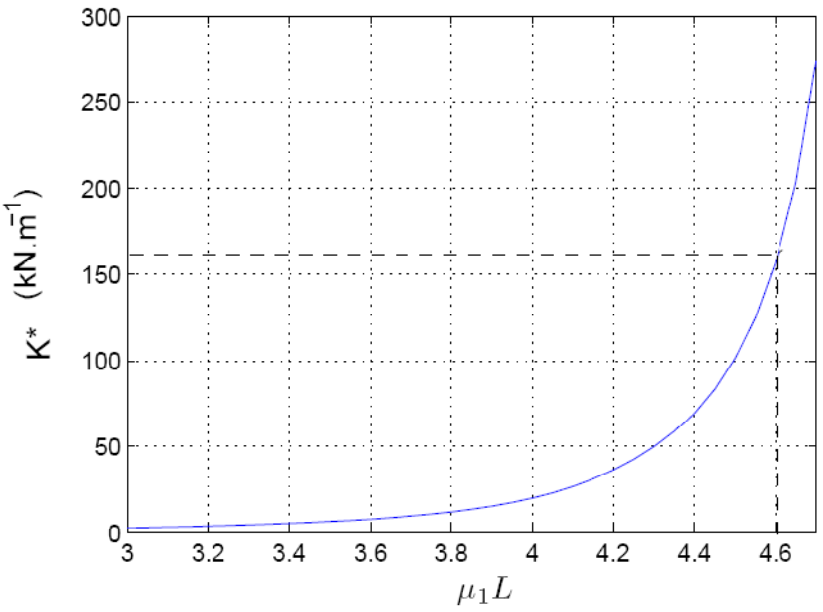

Figure 5: Example of solution in the case of a silicon sample.

2 Optimization of the SMM

2.1 – The theoretical study

In this part we present the study of the sensitivity optimization of our system the SMM. The flexural contact modes of vibration of the cantilever have been modeled. We discuss the matching between the cantilever stiffness and the contact stiffness which depends on the sample material. In order to obtain the best sensitivity, the stiffnesses must be the closest one to each other. Because the length of the cantilever directly affects its stiffness, the cantilever geometry can be optimized for different materials. We have validated this study with measurements on a soft material the Polydimethylsiloxane (PDMS) with a cantilever optimized for materials of Young's moduli of some megapascals. Experimental results obtained with two different samples have shown the high sensitivity of the method for the measurement of low Young's moduli.[22,23]

The sensitivity of our measurement system can be defined as $\partial f / \partial k^*$ or $\partial f / \partial E^*$ which represents the variation of resonant frequency for a variation of contact interaction or local elasticity. Actually, we need to obtain the greatest shift frequency for two materials of different

Young's moduli. Such considerations have already been treated for AFM in force modulation by Chang,[24] Wu et al.,[25] Turner and Wiehn.[26] For all the sensitivity study we considered that the beam is clamped because the spring k_p modeling the bimorph interaction depends on the cantilever and cannot be applied here. We plotted the normalized sensitivity of the first three flexural modes versus contact stiffness for a beam with a length of 4 mm and with k^*=0.68 k_{lat} (Fig. 6). We can see that for soft materials, the first mode is the most sensitive. But when contact stiffness increases and reaches nearly a hundred times the cantilever stiffness, the second mode becomes the most sensitive. And for larger values of contact stiffness the third mode becomes the most sensitive too. We can also notice that the first mode becomes always less sensitive when the contact stiffness is greater, whereas for the other modes the sensitivity first decreases and increases again to reach a local maximum before decreasing with the contact stiffness. We can also plot the following expression: $S_N = (\partial f / \partial k^*)(k^* / f)$ which represents better the ability to distinguish two different materials with Young's moduli close to each other than sensitivity does. Actually S_N is well appropriate because it takes into account the working frequency and contact stiffness. S_N has been plotted for a cantilever with a length of 4 mm versus contact stiffness (Fig. 7). We can see that the curves are different from those of the sensitivity. S_N has a global maximum, whereas precedent sensitivity always decreases with contact stiffness for the first mode. Besides curves appear quite symmetrical on each side from this maximum. By means of this parameter, we highlight precisely the contact stiffness which maximizes the ability to measure elastically close materials. For the first mode S_N reaches a maximum for a contact stiffness of nearly ten times the cantilever's one, 1000 times for the second mode, and 10 000 times for the third mode. We can also notice that the range of high value of S_N is large for the first mode but is reduced for the second mode and even more for the third one.

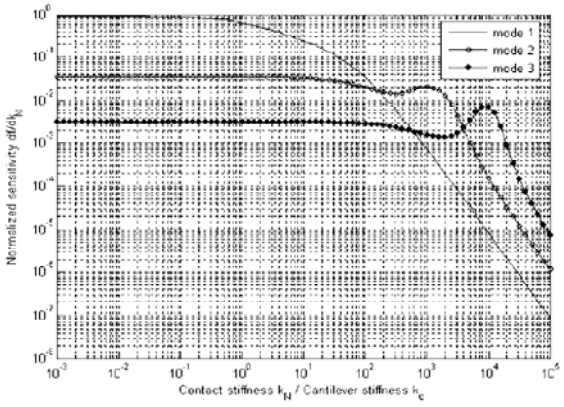

Figure 6: Normalized flexural sensitivity *df* /*dkN* as a function of contact stiffness k^* (normalized by the cantilever stiffness k_c), with k_{lat}=0.68 k^* for a cantilever with a length of 4 mm, a width of 400 µm, and a thickness of 150 µm for the first three modes.

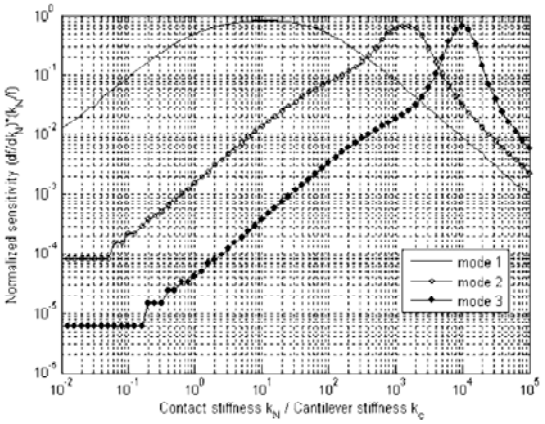

Figure 7: Normalized flexural sensitivity (df/dk^*) x k^*/f as a function of contact stiffness k^* (normalized by the cantilever stiffness k_c), with k_{lat}=0.68 k^* for a cantilever with a length of 4 mm, a width of 400 µm, and a thickness of 150 µm for the first three modes.

In order to have the best sensitivity, the cantilever stiffness k_c and the contact stiffness k^* must be close. In fact, if k^* is far bigger than k_c, the cantilever will totally bend. Whereas if k_c is far bigger than k^*, the tip will indent the sample. The cantilever stiffness k_c equals $3E_cI / L^3$, I being

the area moment of inertia $I=bh^3/12$ for a rectangular section beam, *w* being the width of the beam, and t_c the thickness. Obviously, the parameters which most affect the stiffness are the length and the thickness of the beam because they are cubed in the expression of k_c. Theoretically, the effect of other parameters such as *w*, R, or the tip height *h* are negligible for this application, but no generalization is allowed. So we have only focused our study on the length of the cantilever it is easier and faster to fabricate on the same wafer beams of different lengths than different thicknesses by clean room techniques. We made the sensitivity study for a static force of 0.5 mN. Normalized first flexural mode sensitivity $S_N = (\partial f / \partial k^*)(k^* / f)$ is plotted for beam lengths from 1 to 7 mm and materials of Young's moduli of 10 MPa, 1 GPa, and 100 GPa (Fig. 8). Thickness is assumed to be 150 µm and width of 400 µm. We can notice that, depending on Young's modulus, sensitivity is increasing or decreasing with the length of the cantilever. Actually for a hundred-gigapascal Young's modulus material, the best sensitivity is obtained with a length of 2 mm, whereas for a ten-megapascal Young's modulus one, it is with the length of 7 mm. So the cantilever with a length of 7 mm is optimized to characterize very soft materials. In fact with this cantilever, contact stiffness with Young's moduli of some tens of gigapascals, such as silicon or silica, k^* (≈150 000 N/m) is nearly 1000 times greater than k_c (≈150 N/m). So S_N is a very useful parameter to compare the efficiency of our measurement system for different materials.

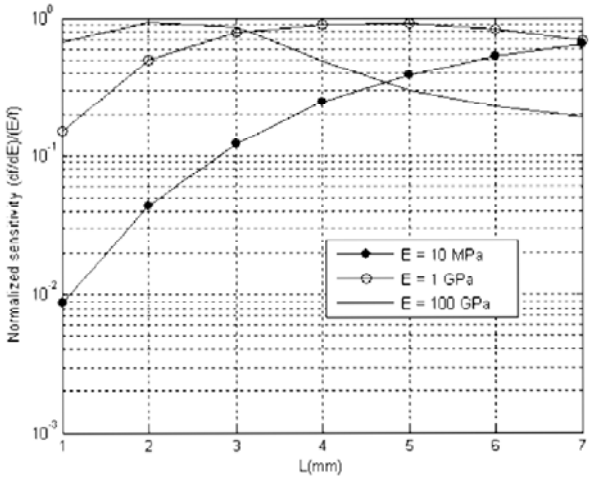

Figure 8: Normalized flexural sensitivity (*df* /*dE*) x *E*/ *f* for a cantilever with a thickness of 150 µm, width of 400 µm for the first contact mode (with a static force of 0.5 mN) as function of the length of the cantilever for different Young's moduli of the sample.

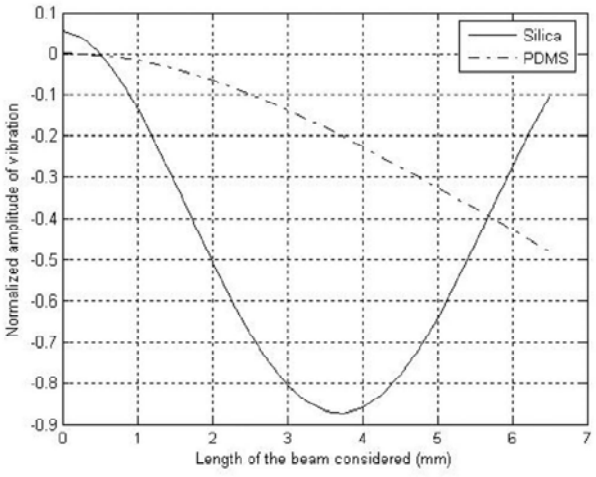

Figure 9: Theoretical deformation shapes of the first flexural mode in contact with SiO2 and PDMS.

2.2 – Experimental validation

We have validated this precedent study by characterizing a very soft material by the cantilever with a length of 7 mm. A sapphire tip with a length of 0.7 mm and a radius of curvature of 45 µm was used. We chose PDMS. PDMS is a silicon-based viscoelastic polymer. Mechanical properties of this material vary with preparation conditions. Actually Young's moduli values can fluctuate in the range of 100 kPa to some megapascals depending on this preparation.[27]

We used two different PDMS samples with thicknesses of some millimeters prepared in different conditions and different aging times. To characterize PDMS we put the spot of the laser at the end of the cantilever because it is where the amplitude of vibration of the first contact mode is the greatest whereas for harder materials the maximum is on the middle of the beam. The model agrees with these observations (see Fig. 9). We can also notice that for hard materials the bimorph interaction spring k_p has a real influence on the modulus computed and has to be fitted with a known sample, whereas with PDMS the value of k_p does not hardly change the result. Figure 10 shows resonances on the first sample of PDMS for different static loads. We can observe the shift frequency and that the amplitude decreases versus the static force because of damping, whereas with an elastic material such as silicon we observed that amplitude increases with the force. To estimate Young's modulus of the sample we realized 15 successive measures in the same conditions. Static force applied was 150 µN because this load provides the best sensitivity (the best slope of frequency versus force). A new contact was obtained for each measurement and we recorded the magnitude spectrum. The dispersion of amplitude is nearly 0.75 Å and 80 Hz in frequency. So we obtain a mean value for the frequency close to 4.18 kHz. And thanks to the model by taking 0.48 for ν, we computed Young's modulus of 3.4 MPa. (±0.3 MPa by considering sensitivity and frequency dispersion). We took 1.7 MPa for the static Young modulus (dynamic mechanical measurement value).

We did the same for our second PDMS sample, and we finally measure a mean resonant frequency of 4.53 kHz and also for Young's modulus a value of 5.5 MPa (±0.3 MPa).

We took 2.8 MPa for the static Young modulus (dynamic mechanical measurement value). The SMM has already been tested on standard hard materials such as silicon and silica[13,20,28] and leaded to a precision of nearly 5% with the model we are using. We are able to characterize two very soft samples with Young's modulus difference of some megapascals. The shift frequency difference between the two materials is 350 Hz (see Fig. 11). For example, the shift frequency difference with the same cantilever between silica (72 GPa) and silicon (100) (130 GPa) is nearly 1 kHz (see Table I). Experimentally the sensitivity has increased by a factor of 10 000. S_N also has increased by a factor of 3.

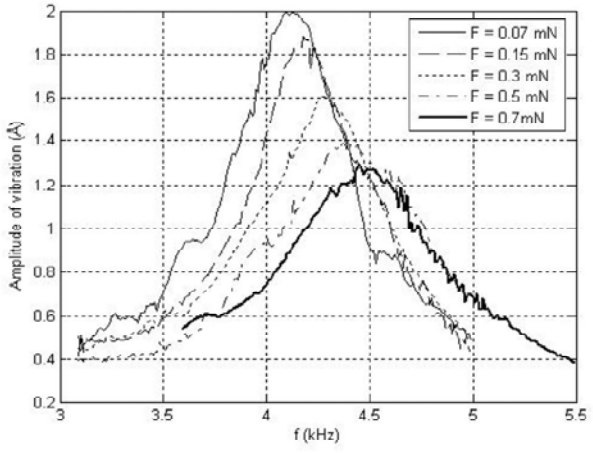

Figure 10: Experimental spectra of amplitude of vibration (first mode) as a function of frequency in contact with the first PDMS sample for a driving

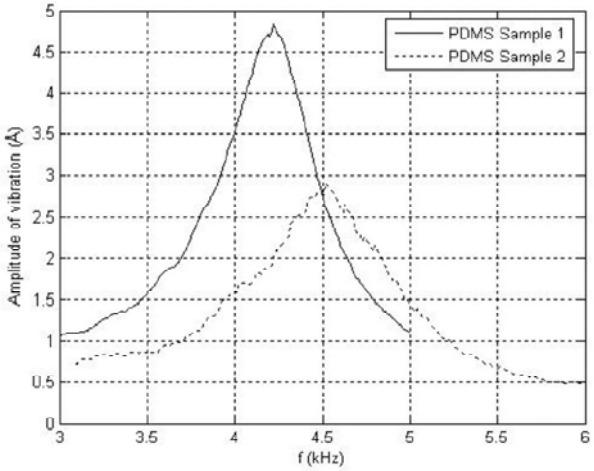

Figure 11: Experimental spectra of amplitude of vibration (first mode) as a function of frequency in contact with the two different PDMS samples for a

voltage of the bimorph of 0.5 V and for different static forces.

static force of 150μN and for a driving voltage of the bimorph of 1 V.

TABLE I

Frequency shifts and sensitivities for stiff and flexible materials with a cantilever with a length of 7 mm.

Materials	SiO_2/Si	Different PDMSs
Δ shift frequency	1 kHz	350 Hz
Sensitivity	0.015 Hz/MPa	167 Hz/MPa
S_N	$47x10^{-3}$	$136x10^{-3}$

2.3 New cantilever geometries

One of the major issues in scanning force microscopy is the application of tangential forces between the tip and the sample during contact. Actually when tangential force becomes too high, the tip slides on the surface (Fig. 12). This leads to prevent a good localization of the measurement and to limit the quantification of the local contact stiffness.

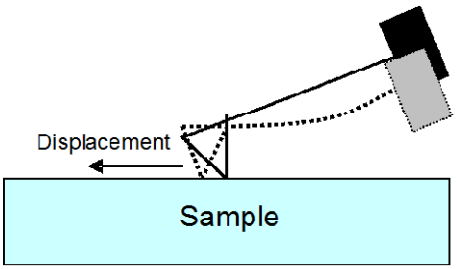

Figure 12: Illustration of the sliding of the tip on the surface during contact.

In atomic force microscopy, stick & slip can occur. The tip alternately sticks and slides on the surface when the force is too high. In dynamic mode, non linearities can appear in the contact resonance curves indicating a loss of contact stiffness, for example in lateral force microscopy [29].

Specific geometries of resonant cantilevers for scanning force microscopy aimed to reduce sliding between tip and sample have been designed and studied. These cantilevers have been designed for the SMM.

With a classic rectangular cantilever, dynamic sliding can be observed on the contact resonance curves. Actually when excitation voltage V_{exc} becomes too high, non linearities appear.

The amplitude of vibration doesn't increase linearly with the excitation and the resonance frequency decreases (Fig.13). It can be explained by the loss of lateral contact stiffness due to sliding.

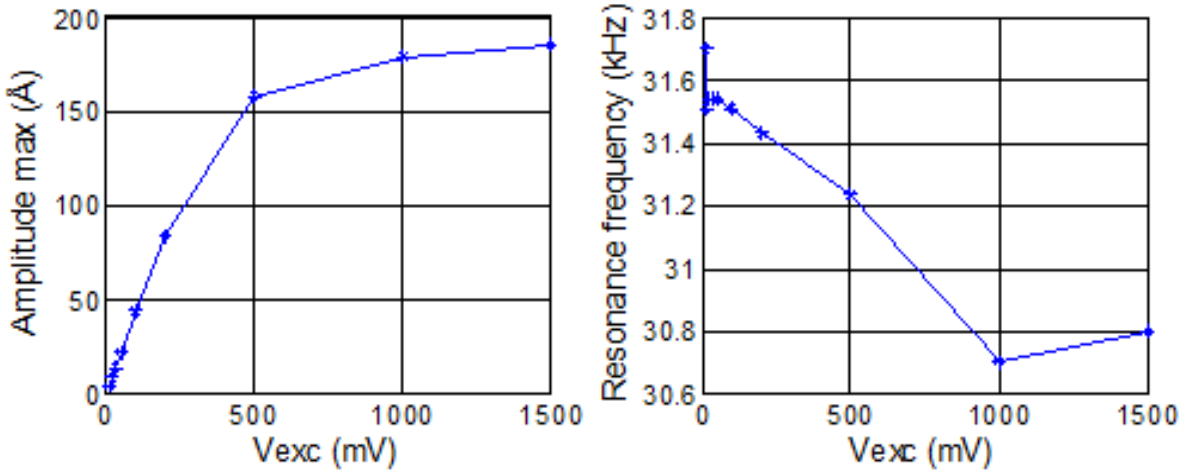

Figure 13: Evolution of the amplitude of vibration and the resonant frequency as a function of the excitation voltage.

Sliding can be reduced by increasing the static force applied and by using a stiffer cantilever but still occurs for a bit higher amplitude of vibration. The underestimation of the contact stiffness leads to limit the quantification of the local elastic constants. So we have thought to specific geometries of resonant cantilevers to prevent the tip from sliding on the surface.
A W-shaped cantilever has been imagined, using a simple mechanism of correction, to keep the tip vertical during contact (Fig. 14). The tip is located on the center of the cantilever. Actually by choosing an appropriate ratio between the lengths l_1 and l_2, the two beams exactly compensate the flexion of the cantilever.

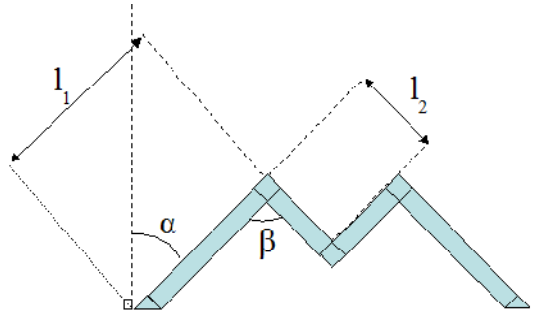

Figure 14: Scheme of the geometry of the new cantilevers conceived.

The conception has been realized thanks to ANSYS software. A parametric study has been made. The thickness of the cantilevers and the width of the beams have been kept constant (respectively 150 µm and 400 µm). The other parameters have been modified and the tip torsion and the stiffness of the cantilever have been recorded. This has enabled us to choose 10 different geometries optimized to prevent sliding and with stiffnesses from 500 N/m to 150000 N/m (Fig. 15). Different stiffnesses have been chosen to optimize the sensitivity to the local contact stiffness depending on the material thanks to the precedent optimization study .

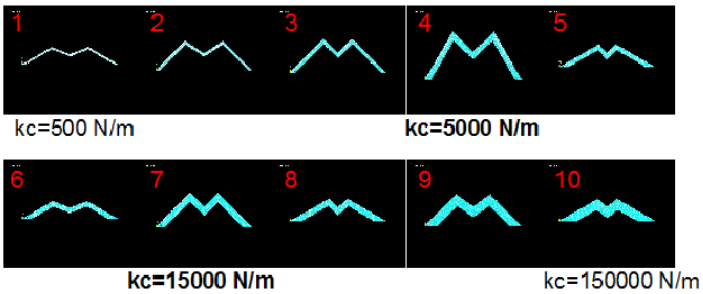

Figure 15: Geometries of the 10 W-shaped cantilevers conceived with ANSYS.

The cantilevers have been fabricated with KOH attack and DRIE process. It has enabled us to obtain satisfying vertical sides (Fig. 16).

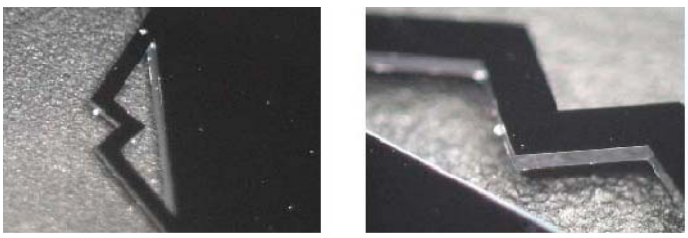

Figure 16: Photography of one of the fabricated W-shaped cantilevers.

i) Static deflections: The static deflections of two Wshaped cantilevers (W4 and W7) have been measured on a silicon surface thanks to the deflectometer and we have compared them to those obtained with a classic cantilever (Fig.17). Actually W-shaped cantilevers have shown deflections 10 to 20 times lower than the classic ones, indicating that the tip remains almost vertical during contact. It can be assumed that the displacement of the tip on the surface has been reduced.

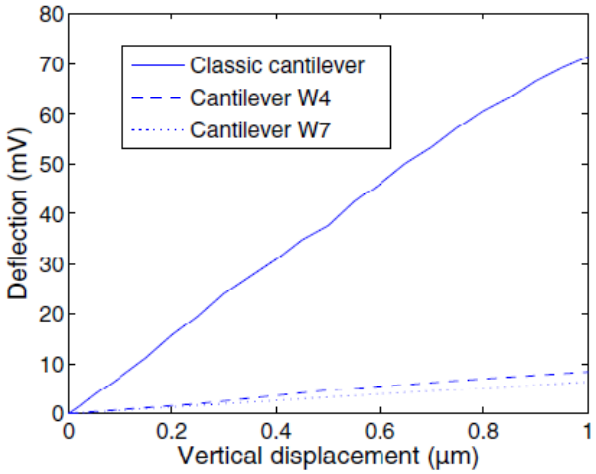

Figure 17: Static deflections measured for two W-shaped cantilevers and for a classic one on a silicon surface.

Finite Element simulations have confirmed these measurements by using the software LS-DYNA. LS-DYNA simulations have shown that while lateral displacement on the surface is important with a classic cantilever (120 nm for a static displacement of 1 µm on a silicon surface), it is 6 to 7 times lower with a W-shaped cantilever. These simulations have confirmed the static satisfying behaviour of our new cantilevers. The tip remains vertical, so it is always the same area of the tip which is put in contact and the lateral displacement is very reduced enabling a good localization of the measurement.

ii) Vibration modes: The W-shaped cantilevers have been excited thanks to a piezoelectric ceramic. Free flexural and torsional vibration modes have been observed and compared to FEM simulations.

Figure 18 gives for example the spectrum of the cantilever W4.

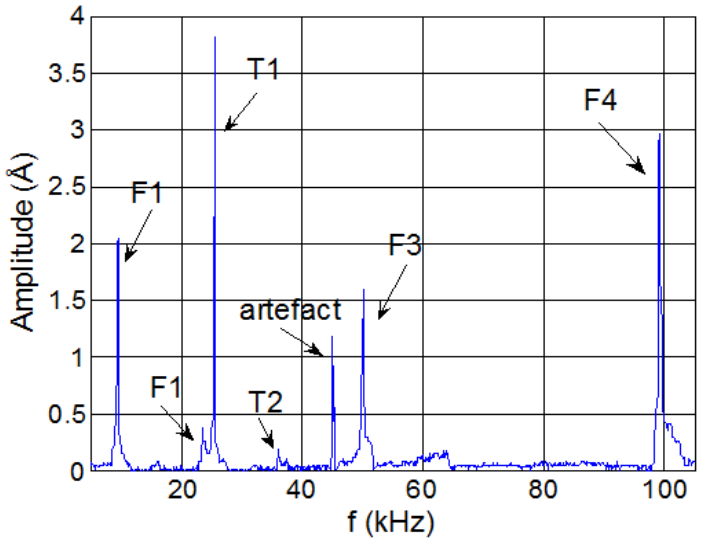

Figure 18: Free amplitude of vibration of the cantilever W4 as a function of the frequency (kHz). Flexural and torsional modes can be observed.

TABLE II compares the experimental measured frequencies and the FEM computed ones. Flexural and torsional modes have easily been observed by the same excitation. A good agreement has been obtained for the first modes but less accuracy with higher modes.

TABLE II
Free vibration modes of the w-shaped cantilever w4

Mode	Experimental frequency (Hz)	FEM computed frequency (Hz)
Flexion 1	9324	9705
Flexion 2	25325	24497
Torsion 1	25300	25579
Torsion 2	35928	41505
Flexion 3	50100	59873
Flexion 4	99200	82765

The contact modes have also been measured on silica and silicon surfaces. The best sensitivity has been obtained for the cantilever W7. The contact resonance curves can be seen in Fig. 19. A good frequency shift has been seen between the two materials. So it has been shown that these cantilevers enable mechanical characterization.

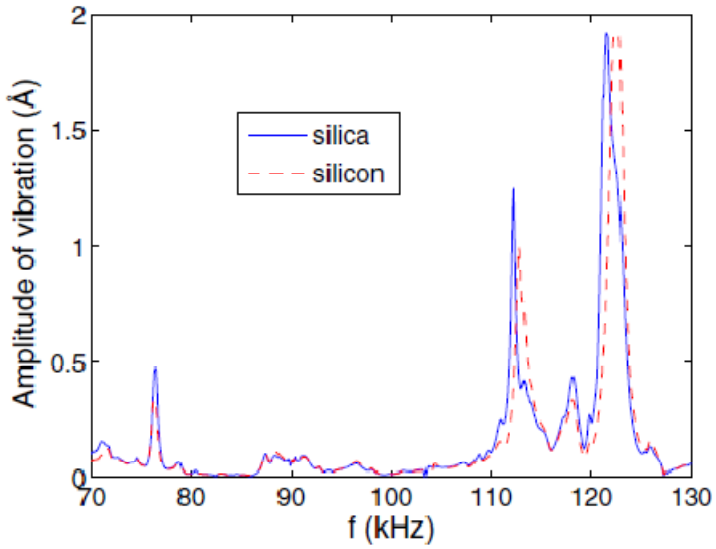

Figure 19: Amplitude of vibration as a function of the frequency, on silicon and silica surfaces, for the W-shaped cantilever W7, for a static force of 7.5 mN.

An even much better sensitivity has also been observed for a higher static force, especially for the torsional modes (Fig.20).

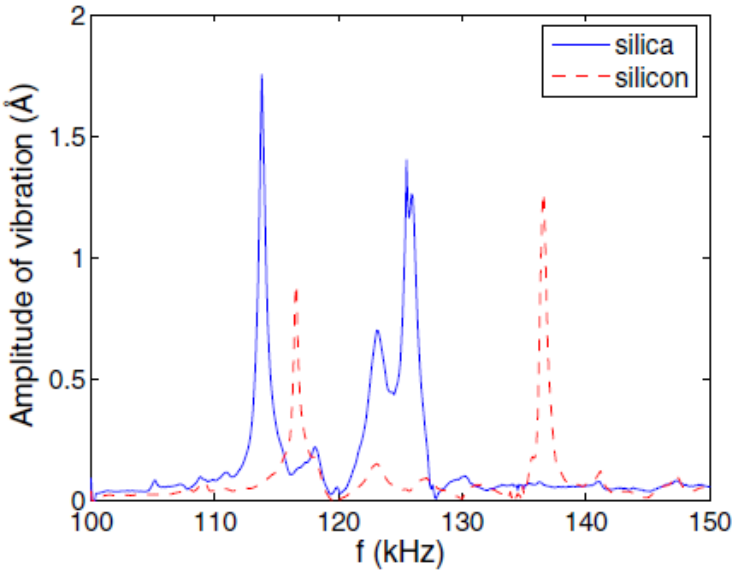

Figure 20: Amplitude of vibration as a function of the frequency, on silicon and silica surfaces, for the W-shaped cantilever W7, for a static force of 15 mN.

LS-DYNA simulations have been realized and have shown a good accuracy for the first flexural mode but far less for the following modes (TABLE III).

TABLE III
Comparison experiment/fem simulations for the vibration modes of the w-shaped cantilever w7 in contact with a silicon surface and for a static force of 7.5 mN.

Mode	Experimental frequency (Hz)	FEM computed frequency (Hz)
Flexion 1	76400	72050
Torsion 1	112300	84714
Torsion 2	121550	90874

iii) Dynamic sliding: Finally to verify the dynamic behaviour of the W-shaped cantilevers the contact resonance curves have been measured for an increasing excitation voltage (Fig. 21). It can be seen that the resonance curves for the flexural mode are quite symmetric. The resonance frequency is constant even for high amplitudes of vibration. This means that dynamic sliding is reduced and it confirms the ability of the W-shaped cantilevers to prevent the tip from sliding on the surface during oscillations. But it can be observed that non linearities appear on the torsional mode, which indicates that there is sliding. It is normal because the W-shaped cantilevers are designed to prevent the tip from sliding in the length direction but not from left to right.

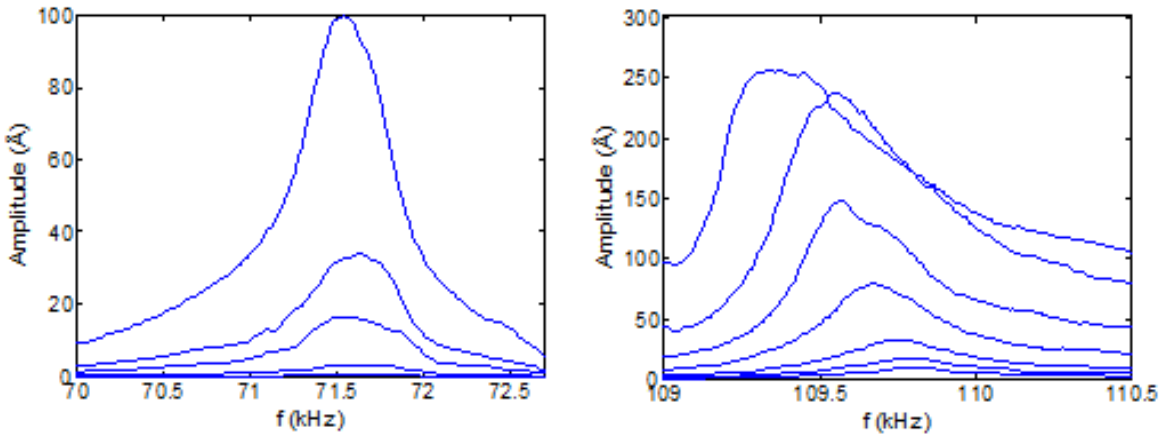

a) b)

Figure 21: Contact resonance curves on a silicon surface of the W-shaped cantilever W7, for a static force of 1.5 mN, for an increasing voltage. **a)** Evolution of the flexural mode, **b)** Evolution of the torsional mode is on the right.

The efficiency of the W-shaped cantilevers to reduce sliding, both in static and dynamic behaviors, has been shown in this paragraph. These cantilevers have exhibited a good sensitivity enabling mechanical characterization. The contact behavior modeling (requiring a numeric solving because of the complex shape) is quite delicate but has provided a good accuracy for the first mode.

3 - Applications on polymers

In the field of materials sciences it is quite hard to have matching mechanical characterization methods at very small scale. This has become possible only in the last few years especially thanks to scanning probe microscopy and nanoindentation [18,30,31]. Viscoelastic properties of polymers have also been measured for low frequencies and for higher frequencies thanks to the time temperature equivalence [32]. Yet, direct measurements at high frequencies are far less studied in the literature of materials.
In this last part, three techniques of dynamic mechanical characterization working at different scales have been used. A Dynamic Mechanical Analysis (DMA) is a technique working at macro scale by tensile tests, The SMM and at last, nanoindentation tests which can characterize materials at nano or micro scale and for quasi-static or dynamic loadings have been carried out [33]. We decided to characterize two polymers by measuring their complex Young's moduli for a wide range of frequencies to exhibit their viscoelastic properties. We chose two very different organic materials often used in MEMS applications, PDMS and SU8 resin. PolyDiMethylSiloxane (PDMS) is a silicon-based elastomer. Mechanical properties of this very versatile material vary with preparation conditions. Young's moduli values can actually fluctuate in the range of 0.1 MPa to some tens of MPa depending on its preparation [35–38]. It exhibits important viscoelastic behaviour. The other material we decided to characterize is a SU8 resin film. This resin is a polymer based on epoxies which is used for photolithography and MEMS applications and has a Young modulus in the range 3–6 GPa associated with a low viscoelastic behaviour [38]. Bulk samples have been designed to allow DMA measurements and to verify the compatibility of these techniques. To our knowledge such a comparison on viscoelastic materials has not been yet reported in the literature. This is the principal aim of this study performed on these two very different polymers.

3.1 - Materials and experimental procedures

i) Materials

Polydimethylsiloxane (PDMS) has become the most popular building material used in a variety of low-cost aqueous microfluidic devices aimed in particular at single use for biological or medical diagnostics. In order to have low power consumption, many groups use this material for the manufacture of mobile part (often membrane, bridge…) in active systems such as microvalves and micropumps. Therefore the characterization of the dynamic mechanical properties of PDMS is of great interest.
Different samples have been tested. Specimen 1 was tested thanks to the three different techniques for aging times t_v of about 1500 h and 11 000 h at constant temperature T ≈ 20–22 ◦C in a closed Petri dish and without light exposure. Specimen 2 is a very old sample which has been aging for a long time (t_v > 3 years) at room temperature (20 to 30 ◦C), without any particular precaution and whose preparation conditions are not exactly the same as those previously presented for specimen 1. Thus, these two PDMS samples must be considered as two different materials. The SU8 resin is a negative epoxy type photoresist

which has been developed by IBM (Watson Research Center). This polymer is a good material for MEMS applications.
Two different samples have been tested. Specimen 1, tested with the three techniques, is a film 0.13 mm thick obtained by spin-coating liquid SU8 resin (for 30 s at 5000 rpm/s) on a glass substrate. Specimen 2 is a film of 50 µm thick deposited on (100) silicon substrate. Due to the small thickness of these films, only nanoindentation and SMM procedures have been carried out.

ii) Dynamic Mechanical Analysis (DMA)

DMA measures with frequencies in the range of 10^{-2} – 100 Hz were performed on a commercial BOSE Electroforce 3200 machine, at room temperature for the three different materials and at T = 23, 0, -20, -40, -60 °C for the PDMS sample 1. Thus, for this specimen the time-temperature equivalence has been analyzed over a large domain of frequency; $10^{-2} < f < 10^{5}$ Hz.

For PDMS and SU8 resin (specimen 1) samples, gage lengths of the specimens were about 30 mm and 36 mm for a cross section of about 13 x 3-4 mm^2 and 10.2 x 0.13 mm^2 respectively. A control on the position with a peak to peak amplitude of 0.5 mm (corresponding to a strain of $\pm$ $7.6.10^{-3}$) for a preload strain of $9.1.10^{-3}$ was realized. Thus the samples were always in tension even at the low point of the cycles. According to the ASTM Standard Guide for Dynamic Testing the software calculates the phase angle ϕ between the imposed displacement and the measured force and uses the specimen shape to convert the stiffness and the phase information to provide the values of E', the storage modulus, E", the loss modulus and tan(ϕ), the tangent of the phase angle. Moreover, for the specimens 1 (PDMS and SU8), the evolution of E' and E" with the aging time t_v has been studied between 3 to about 1300 hours.

iii) Nanoindentation tests

The Berkovich's indentations were performed with a Nanoindenter IIS (NanoInstruments). The hardness H_b and the Young's modulus $E*$ are deduced using the classical static procedure or the continuous stiffness method (CSM). One of the most commonly used methods for analysing nanoindentation data is the Oliver and Pharr one [30], which expands on earlier ideas developed by Loubet et al. [39] and Doerner and Nix [40]. This analysis has often been applied to polymer characterization, for example [38], [41] and [42], even if the true contact area is underestimated due to the pushing up of the material around the indenter. In this case the Young's modulus is slightly overestimated. However, in our method the Young's modulus has been estimated for an indentation depth close to zero and thus the pile up effect may be considered as negligible.
In the CSM method a small harmonic load oscillation is superimposed to the static one and if the tested material presents a viscoelastic character it is then possible to deduce its complex modulus [43]. If the dynamic loading is given by:

$$F = F_0 \exp(i\omega t) \tag{16}$$

the deformation response of the material is:

$$\Delta h = \Delta h_0 \exp(i\omega t)\exp(i\phi) \tag{17}$$

where ϕ is the phase lag due to viscous dissipation, as for the SMM technique. The components of the complex modulus E* can be calculated according to:

$$E'^* = S_d \frac{\sqrt{\pi}}{2\eta\sqrt{A}} \cos(\phi) \tag{18}$$

$$E''^* = S_d \frac{\sqrt{\pi}}{2\eta\sqrt{A}} \sin(\phi) \tag{19}$$

with $S_d = F_0/\Delta h_0$, A_p the projected area of the elastic contact, η = 1.034 for a Berkovich's tip and thus $\tan(\phi) = E''^*/E'^*$.

Nanoindentation tests were performed using a Nanoindenter IIS. As previously mentioned the study was conducted following the classical (quasi-static) and CSM (dynamic at f = 45 Hz) procedures. For each tested sample and for each initial stiffness S_0, the measurement sequence consists of 5 indents with a 50 µm space between them with a maximum penetration depth of h_{max} = 4 µm. The penetration speed was not constant but increased with depth from 2 to 45 nm s^{-1} with 8 steps such that $\dot{\varepsilon} = (1/h)(dh/dt)$ is approximately constant and equal to 2 × 10−2 s^{-1}. The stiffness of the indentation cell S_i is 44 N/m and the values of the imposed initial stiffness are in the range 53 < S_0 < 94 N/m. For the quasi-static method, four unloadings (to 90% of the total loading) were performed at about h_{max} ≈ 1, 2,3 and 4 µm and 50% of the unloading curves are considered to calculate the contact stiffness of the samples. For the CSM procedure, the indenter vibrates at a frequency of 45 Hz for amplitude of 1–2 nm during the indenter penetration ($\dot{\varepsilon} \approx 2 \times 10{-}2\ s^{-1}$).
In the case of the SU8 films the maximum penetration depth has been fixed at h_{max} = 3 µm and the contact between the surface of the sample and the indenter tip is easily detectable. Thus, the measured values of the Young's modulus and of the hardness are constant overall the indentation depth.

iv) The SMM

In this study a simple spring-mass approximation has been introduced to take into account the damping and to determine the complex Young's modulus like Arinéro et al. [44] did for an AFM. First, the relation between the frequency f_0 and *k** is obtained:

$$f_0 = \frac{1}{2\pi}\sqrt{\frac{k^* + k_c}{m_{eff}}} \tag{20}$$

where k_c is the beam stiffness. The linear differential equation describing the response of an oscillator, with m_{eff} the effective mass of cantilever and tip, $\tilde{x}$ the complex value of the response, ω_0 the cantilever-tip-sample system's resonance angular frequency and λ the damping coefficient is:

$$\frac{\partial^2 \tilde{x}}{\partial t^2} + 2\lambda \frac{\partial \tilde{x}}{\partial t} + \omega_0^2 \tilde{x} = \frac{F_0}{m_{eff}} \exp(i\omega t) \tag{21}$$

with: $\tilde{x} = X_0 \exp(i\omega t) \exp(i\phi)$.

So,

$$X_0 \exp(i\phi) = \frac{F_0 / m_{eff}}{(\omega_0^2 - \omega^2) + 2i\omega\lambda} \tag{22}$$

Introducing the resonance frequency of the system f_0 and the 3 dB half-bandwidth f_1, given by $f_0 = \omega_0/2\pi$ and $f_1 = \lambda/2\pi$, the expression of the complex contact dynamic stiffness can be obtained:

$$k_{CCD} = \frac{F_0}{X_0 \exp(i\phi)} = m_{eff}\,(4\pi^2(f_0^2 - f^2) + 8i\pi^2 f\, f_1) \tag{23}.$$

By taking the imaginary part, and as f is close to f_0, the k''^* stiffness is obtained:

$$k''^* = 8 m_{eff} \pi^2 f_0 f_1 \tag{24}$$

Introducing the complex effective Young modulus E_x^*:

$$E_x^* = E'^* + iE''^* \tag{25}$$

and writing the expression of the complex stiffness as [45]:

$$k^* = k'^* + ik''^* \tag{26}$$

with a static Hertz contact:

$$k''^* = E''^{*2/3}(6RF_0)^{1/3} \tag{27},$$

and thanks to Eqs. (20), (24) and (27), the expression of E''^* is given by:

$$E''^* = \frac{(2(k'^* + k_c)f_1)^{3/2}}{f_0^{3/2}(6RF_0)^{1/3}} \tag{28}$$

This relation will be used for the SU8 resin as $E_1^* \approx E_0^*$.

For a dynamic contact:

$$k^{*''} = \frac{E_1^{''*}}{E_0^{*1/3}} \left(6RF_0\right)^{1/3} \tag{29}$$

Thanks to Eqs. (20), (24) and (29), the following expression of $E_1^{''*}$ has been obtained:

$$E''^* = \frac{2(k'^* + k_c) f_1 E_0^{*1/3}}{f_0 \left(6RF_0\right)^{1/3}} \tag{30}$$

This relation will be used for the PDMS elastomer.

At last, it is interesting to note that the relations on the components of the complex Young's modulus determined with the hypothesis of static (st) (Eq. 1) or dynamic (dyn) (Eq. 2) Hertz contact are such that :

$$E_{dyn}^{'*} = (E_{st}^{'*})^{2/3} E_0^{*1/3} \quad \text{and} \quad E_{dyn}^{''*} = (E_{st}^{''*})^{2/3} E_0^{*1/3} \tag{31}.$$

It is thus possible to write:

$$E_{dyn}^{(i)*} = E_{st}^{(i)*} \left(\alpha + (1-\alpha) \left(\frac{E_0^*}{E_{st}^{(i)*}} \right)^{1/3} \right) \tag{32}$$

with (i) = (' or "), α = 1 for a non viscous material and α = 0 for a viscoelastic material.

Two different cantilevers have been used for the characterization of these two materials. Thanks to the previous study on the sensitivity of the SMM, we chose 2 different cantilevers which are optimized for PDMS and SU8 resin. Actually, we showed that the cantilever stiffness must be chosen close to the contact stiffness to have the best sensitivity. As cantilever stiffness depends on the inverse of the cube of the length, a length of 7 mm for PDMS and 4.5 mm for the SU8 which is harder have been chosen. The width and the thickness of the beam are 400 µm and 150 µm respectively. The tip has a cylindrical base and a conical end as shown in Figure 1. The sharp end of the tip is spherical. For the beam with a length of 7 mm, the tip length l is 697 µm, its mass m = 0.23 µg and its curvature radius R = 45 µm. For the one with a length of 4.5 mm, l = 976 µm, m = 0.45 µg and R = 20 µm. The static applied force F_0 was 0.15 mN for the PDMS and 0.5 mN for the SU8 resin. The frequency domain of the SMM with these cantilevers corresponds to some kHz.
With these experimental conditions the polymers are loaded in their linear viscoelastic regime. Actually, PDMS remains linear until deformations of 60% [37] and 5% for SU8 resin [38]. For a spherical tip like SMM ones, deformation of the contact area is $\varepsilon = 0.2\, a_c/R$ [46], where a_c is the contact area radius and R the tip radius. With the tips we have used, a_c < 5 µm and R > 20 µm, thus ε < 5%.

3.2 Experimental results

The three techniques work at different scales and at different frequencies. As previously shown, they enable us to check the viscoelastic properties of these polymers. Actually, storage and loss moduli of polymers change depending on the frequency. We recorded the measures of E' and E" for the two specimens of PDMS and for the two SU8 resin films.

i) Phenomenological modelling

From a material point of view and for viscoelastic materials as polymers, the crucial problem in vibration experiments concerns the accurate determination of the viscoelastic parameters over a broad range of frequency. So, in the case of sinusoidal deformation, the complex modulus can be written as [47]:

$$E^* = E^i + (E^r - E^i) \sum_{j=1}^{n} p_j \frac{1}{1+i\omega\tau_j} \quad \text{with} \quad \sum_{j=1}^{n} p_j = 1 \tag{33}$$

where E^i and E^r are the instantaneous and relaxed Young's moduli, respectively. The parameters τ_j are the different relaxation times and p_j is a ponderation coefficient for each relaxation time. It is very difficult to determine the values of the parameters p_j, τ_j and their number n. From a phenomenological point of view, to overcome this difficulty the empirical model of Havriliak and Negami [48] (H-N model) is considered, which combines the advantages of the modelling of Cole et al. [49] and Davidson et al. [50]. In this model, the complex modulus is given by:

$$E^* = E^i + (E^r - E^i) \frac{1}{(1+(i\omega\tau)^\alpha)^\beta} \tag{34}$$

Thus, storage and loss moduli are respectively given by:

$$E' = E^i + (E^r - E^i) \frac{\cos(\beta\phi)}{\left(1+2(\omega\tau)^\alpha \cos(\alpha\pi/2) + (\omega\tau)^{2\alpha}\right)^{\beta/2}} \tag{35}$$

$$E'' = (E^i - E^r) \frac{\sin(\beta\phi)}{\left(1+2(\omega\tau)^\alpha \cos(\alpha\pi/2) + (\omega\tau)^{2\alpha}\right)^{\beta/2}} \tag{36}$$

$$\text{with} \quad \phi = \tan^{-1}\left(\frac{(\omega\tau)^\alpha \sin(\alpha\pi/2)}{1+(\omega\tau)^\alpha \cos(\alpha\pi/2)}\right) \tag{37}$$

where τ is a single parameter with time dimension and α, β two empirical parameters.

Note that if $\alpha = \beta = 1$, the equation (35) with a single relaxation time is obtained. The different experimental curves of Figs. 22, 23 and 24 for the PDMS and Figs. 25, 26 and 27 for the SU8 resin have been fitted by equations (35), (36), (37) and the results drawn on these figures. The identified values of the parameters are listed in Table IV. Note that these values

correspond to the working range of frequencies and cannot be used for very higher frequencies.

TABLE IV
Parameters values of equations (33) (34) and (35)

Specimen	t_v	α	β	τ	E^r(MPa)	E^l(MPa)	F(Hz)
PDMS (Spec.1)	1460 h	0.236	1	$2x10^{-9}$	1.65	29.6	10^{-2}-10^{6}
PDMS (Spec.2)	>25000 h	0.236	1	$2x10^{-9}$	2.6	44	10^{-2}-10^{6}
SU8 (Spec.1)	1000h	0.4	0.38	40	3600	4500	10^{-2}-10^{5}
SU8 (Spec.2)	1000h	0.4	1	0.5	5000	5600	10^{-2}-10^{5}

ii) Case of the PDMS samples

We took ν = 0.48 for the Poisson's ratio of the PDMS (hyperelastic material). The values of E' for the two PDMS samples are plotted in Fig. 22 as a function of the working frequency and for the three experimental techniques. Note that for the SMM value, f is the first contact resonance frequency equals to 4.18 KHz. The measures given by the DMA and the nanoindentation methods are in a fairly good agreement. The SMM ones even if it is two decades further show a possible continuity. Static moduli E_0^* for the two samples are respectively 1.7 and 2.9 MPa. As it will be shown, this difference is principally due to the different preparation conditions and weakly to the aging time. Storage modulus increases with the frequency for the two samples, which is typical of a viscoelastic material. For these two materials the values given by the SMM at nearly 4 kHz are 3.4 and 5.5 MPa (Fig. 22). In the Fig. 23 the loss modulus is plotted as the function of the working frequency. At 0.01 Hz the values are very low, near zero, but sharply increase with the working frequency. Results between DMA and SMM show the same behaviour for E" than for E'. Typically, for polymers, E" increases before reaching a maximum and then decreases with the working frequency. The SMM values of E" at 4 kHz for the two specimens are about 1 and 1.6 MPa.

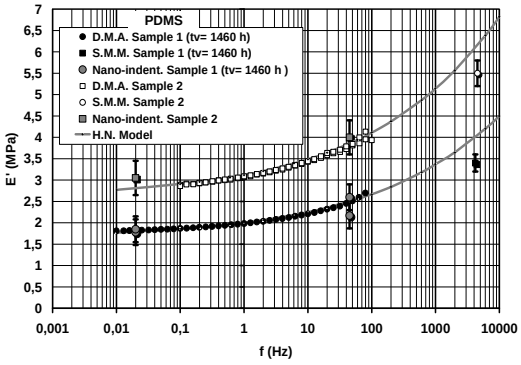

Figure 22: Storage modulus of PDMS samples measured by nanoindentation, DMA and SMM techniques as a function of the working frequency. Simulation with the H-N model.

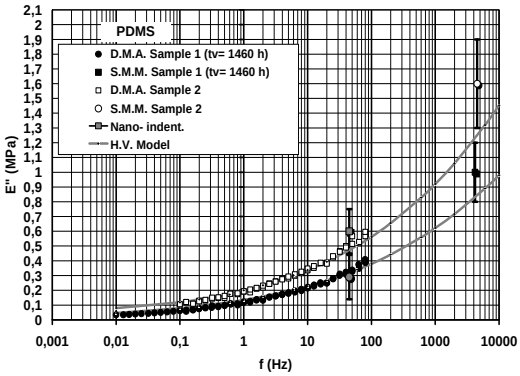

Figure 23: Loss modulus of PDMS samples measured by nanoindentation, DMA and SMM techniques as a function of the working frequency. Simulation with the H-N model.

E' and E" are of the same order of magnitude which means that for this range of frequencies the material is very viscoelastic. This behaviour is quantified by the parameter tan(ϕ) = E"/E' as shown in Fig. 24. The values estimated with the CSM nanoindentation procedure are in good agreement with those obtained by the DMA analysis. The SMM values also show a possible continuity. The tan(ϕ) parameter is an increasing function of the frequency, as expected, and the SMM values are close to 0.28 for f $\approx$ 4 kHz. It should then decrease for higher frequencies; the maximum value should be obtained at a frequency of about 10^6 Hz. From a material point of view, it is interesting to note that the values of the tan(ϕ) parameter are the same for the two tested specimens, indicating that this parameter seems insensitive to the elaboration conditions and the aging time as it will be shown later.

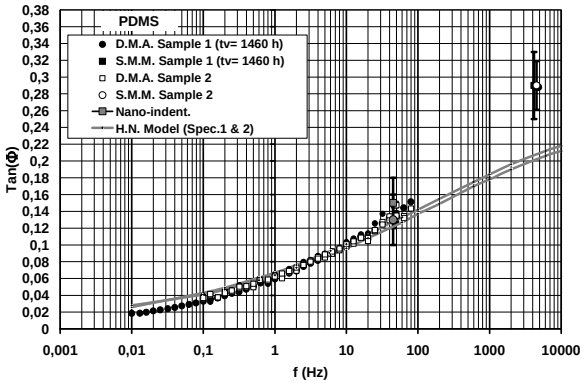

Figure 24: tan(ϕ) parameter of PDMS samples determined by the three different techniques. Simulation with the H-N model.

iii) Case of the SU8 resin

The same measures on the SU8 resin film have been carried out. For this material we took a Poisson's ratio of ν = 0.29. For the two specimens the evolution of the storage modulus E' with the frequency has been plotted in Fig. 25. This time, the three techniques do not perfectly match. Actually for sample 1, at 0.01 Hz the DMA value is about 2.9 GPa (2

different measures) whereas the nanoindentation value is about 4.5 GPa. Moreover, for these two techniques the storage modulus slightly increases with the frequency in the studied range. The SMM value at 23 kHz (first resonance frequency) confirms the indentation modulus values with a nearly equal value of 4.2 GPa. As previously mentioned, the value of the order of 4.5 GPa is in agreement with the results given in the overall literature E' ≈ 4 to 6 GPa. The low values obtained by DMA technique are certainly due to the too small thickness of the tested specimen (0.13 mm) and the small preload strain (≈ 9.10^{-3}) allowing to a certain inhomogeneity in the strain field across the specimen section. The artefacts due to the instrument compliance effects observed on rigid specimens are also not neglectible. So in the typical curve of the storage modulus of a polymer, the maximum of slope has already been passed and the modulus is quite constant. The same evolution can be expected for the loss modulus in this range of frequencies. In Fig. 26 a loss modulus which decreases with the frequency can be observed. The nanoindentation value is a slightly greater than the DMA one. The SMM value at 23 kHz is lower and confirms the global decreasing of the loss modulus. It can be noted that the loss modulus if far lower than the storage one (20-80 MPa versus 4-4.5 GPa). Thus, the SU8 resin presents very weak viscoelastic behaviour, far less than the PDMS one.

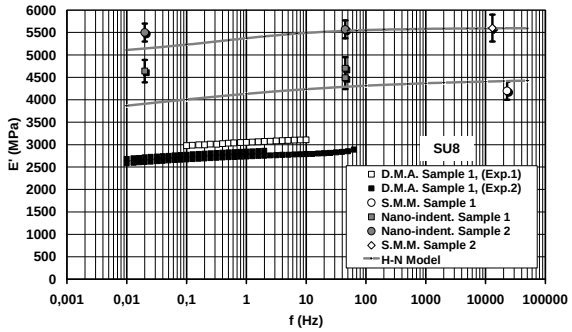

Figure 25: Storage modulus of SU8 resin samples measured with the three techniques as a function of the working frequency. Simulations with the H-N model.

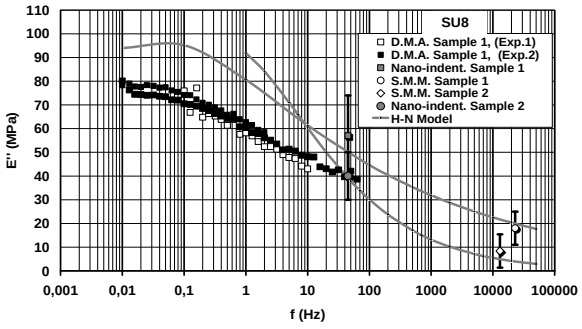

Figure 26: Loss modulus of SU8 resin samples measured with the three techniques as a function of the working frequency. Simulations with the H-N model.

The tan(ϕ) has also been plotted in Fig. 27. The maximum has been passed (f ≅ 10^{-2} Hz) and this parameter decreases with the frequency. Of course, the values are much lower than for the PDMS and the maximum value is close to 0.025. It is important to observe that the three techniques perfectly match. DMA and nanoindentation values are the same at 45 Hz and the SMM value prolongs the decrease of the curve. In fact with DMA technique, the error due to the small thickness of the film (or other causes) has the same effect on the determination of E' and E" and disappears on the loss tangent which is equal to the ratio E"/E'.

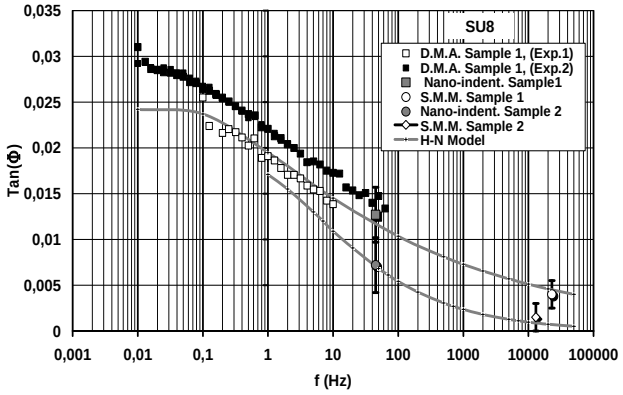

Figure 27: tan(ϕ) parameter of the two SU8 resin samples determined by the three techniques. Simulations with the H-N model.

Nanoindention and SMM measurements have been performed on the same sample (specimen 1) but for an aging time at room temperature of about 13000 h. Contrary to the PDMS samples, no noticeable evolution outside of the method accuracies has been pointed out.

For the SU8 film deposited on the Si substrate (specimen 2), the nanoindentation and the SMM techniques perfectly match (Fig. 25) and the determined values of the storage modulus are 5.57 $\pm$ 0.15 GPa and 5.6 $\pm$ 0.3 GPa, respectively. These values are higher than those measured on specimen 1, but close to those reported by Al-Halhouli et al. [38], i.e.: 5.2 GPa. The values of the loss modulus and the tangent of the phase lag are plotted in Figs. 26 and 27. As for the specimen 1 these two parameters decrease with the frequency, but the values are slightly lower than those determined on the previous sample, i.e.: E''= 40 MPa (at 45 Hz) and E''= 8.4 MPa (at 13 KHz) for the nanoindentation and the SMM procedures, respectively. These observations, increasing of E' and decreasing of E'' compared to the values obtained on sample 1, are certainly due to the long bake during 15 h at 90°C performed on this specimen.

Note that the Berkovich hardnesses H_b of these different polymers are about, H_b = 0.33 $\pm$ 0.05 MPa and 0.55 $\pm$ MPa for the two PDMS samples (specimens 1 and 2 respectively) and H_b = 330 $\pm$ 20 MPa and H_b =362$\pm$ 13 MPa for the two SU8 films (specimens 1 and 2). This last value is in fairly good agreement with the one given by Al-Halhouli et al. [38] ($H_b \approx$ 430 MPa).

The simulations are fairly good especially considering on the one hand the three different experimental techniques that have been used and on the other hand the wide range of frequency which has been analysed. Notice the very great difference between the time parameter of the PDMS and the SU8 resin's one; the PDMS is very viscous (tan(ϕ) $\approx$ 0.21 at f = 10^4 Hz) contrary to the SU8 resin (tan(ϕ) $\approx$ 0.005 at f = 10^4 Hz for sample 1). The same

trend is observed on the ratio between the instantaneous and the relaxed moduli, E^i/E^r: $E^i/E^r \approx 17$ for the PDMS and only ≈1.12-1.25 for the SU8 resin.

- Conclusion

In this chapter we have presented different new trends concerning the field of micro and nanocharacterization with near-field microscopes, focalized on the behaviour of the SMM. Neither less all the conclusions summarize below can be very useful for all these near-field microscopes.

Optimization of the SMM by taking into account the sample material considered and the stiffness of the cantilever can be summarize as follows: (i) the sensitivity of the three first contact modes of the SMM has been studied. Sensitivity decreases with the contact stiffness. The first mode is the most sensitive but when contact stiffness increases higher modes become the most sensitive. (ii) The parameter S_N sensitivity reduced to working contact stiffness and frequency shows for each mode a maximum corresponding to contact stiffness. Actually we saw that S_N is maximum when the contact stiffness and the cantilever stiffness are of the same order of magnitude for the first mode. (iii) The sensitivity is also depending on the stiffness of the cantilever. So the length of the cantilever which directly affects its stiffness is a mean to optimize the cantilever with the considered material.

New cantilever geometries (W-shaped) have been investigated and allowing to give these characteristics: (i) The efficiency of the W-shaped cantilevers to reduce sliding, both in static and dynamic behaviours (ii) These cantilevers exhibit a good sensitivity enabling mechanical characterization.

In the last part the efficiency of the three mechanical characterization methods (DMA, SMM, Nanoindentation) has been pointed out. The results of the three different scales techniques (macro, micro and nanoscale) fairly match. The two very different viscoelastic behaviours of PDMS and SU8 resin for the same frequency range have been quantified. Their storage, loss moduli and tan(φ) from 0.01 Hz to some kHz have been measured. Satisfying global behaviours according to the models and good agreement between measured values and literature ones have been obtained. In conclusion, these three complementary experimental techniques can be used as powerful metrology tools for the mechanical characterization at very small scale of viscoelastic materials. To our knowledge, such a comparison of these three experimental methods applied on viscoelastic materials has not been reported in the literature and highlights the potentialities of these techniques for polymer applications.

REFERENCES

[1] Cretin B., Sthal F.,(1993) Appl. Phys. Lett. 62 829-31.

[2] Vairac P., Cretin B., (1996) Appl. Phys. Lett. 68 461-3.

[3] Kolosov O., Ogiso H., Tokumoto H., Yamanaka K., (1994) Springer series in materials sciences 31 345-8.

[4] Rabe U., Arnold W., (1994) Appl. Phys. Lett. 64 1493-5.

[5] Burnham N. A., Kulik A. J., Gremaud G., Gallo P. J., Ouveley F., (1996) J. Vac. Sci. Technol. B14 794-9.

[6] Chilla E., Hesjedal T., Frohlich H. J., (1994) Proc. IEEE Ultrasonics Symposium 363-6.

[7] Maivald P., Butt H. J., Gould S. A., Prater C. B., Drake B., Gurley, J. A., Elings V. B. and Hansma P., (1991), Nanotechnology 2, 103.

[8] Florin E. L., Radmacher M., Fleck B. et Gaub H., (1994), Rev. Sci. Instrum. 65, 639.

[9] Han W. H. Lindsay S. M. et Jing T., (1996), Appl. Phys. Lett. 69, 4111.

[10]Vairac P., (1996), Thèse de l'Université de Franche-Comte, PhD Thesis, Besançon, France.

[11] Cretin B., Vairac P., (1997), Appl. Phys. Lett. 71 2082-84.

[12] Vairac P., Cretin B., (1996), Optic Com.132 19-23.

[13] Cretin B., Vairac P., (1998), Appl. Physics A-Material Science & Processing 66 227-30.

[14] Kolosov O., Yamanaka K, (1993) Jpn. J. Appl. Phys, 32:1095.

[15]Rabe U. et Arnold W. (1994), Appl. Phys. Lett. 64, 1493-1495.

[16] Burnham N. A., Kulik A. J., Gremaud G., Gallo P. J. et Ouveley F. (1996a), J. Vac. Sci. Technol. B 14, 794-799.

[17]E. Dupas, G. Gremaud, A. Kulik, and J.-L. Loubet, (2001) Rev. Sci. Instrum. 72, 3891

[18] X. Li and B. Bhushan, (2002) Mater. Charact. 48, 11

[19] Vairac P. and Cretin B., (1998) Appl. Phys. A: Mater. Sci. Process. 66, 235

[20] Vairac P. and Cretin B., in Scanning Microdeformation Microscopy: Subsurface Imaging and Measurement of Elastic Constants at Mesoscopic Scale, Applied Scanning Probe Methods II, edited by B. Bhushan and H. Fuchs (2006) Springer, Berlin, pp. 241–281.

[21] Johnson K. L., Contact Mechanics (1987) Cambridge University Press, Cambridge,

[22] Le Rouzic J., Vairac P., Cretin B. and Delobelle P., (2008) Rev. Sci. Instrum. 79, 033707.

[23] Le Rouzic J., (2009), Thèse de l'Université de Franche-Comte, PhD Thesis, Besançon, France.

[24]W.-J. Chang, (2002) Nanotechnology 13, 510

[25]T.-S. Wu, W.-J. Chang, and J.-Ch. Hsu, (2004) Microelectron. Eng. 71, 15.

[26] J. A. Turner and J. Wiehn, (2001) Nanotechnology 12, 322.

[27] J. A. Walberer and A. J. McHugh, (2001). J. Rheol. 45, 187.

[28] P. Vairac and B. Cretin, (1999) Surf. Interface Anal. 27, 588.

[29] V. Scherer, W. Arnold, (1997), In: B. Bhushan (ed.) Micro/nanotribology and its applications. Kluwer Academic

[30] W.C. Oliver, G.M. Pharr, (1992), J. Mater. Res. 7, 1563
[31] W.C. Oliver, G.M. Pharr, (2004), J. Mater. Res. 19, 3
[32] C.C. White, M.R. Vanlandingham, P.L. Drzal, N.-K. Chang, S.H. Chang, (2005), J. Polym. Sci. B 43, 1812
[33] Le Rouzic J., Delobelle P., Vairac P. anb Cretin B., (2009), Eur. Phys. J. Appl. Phys. 48, 11201.
[34] J.A. Walberer, A.J. McHugh, (2001), J. Rheol. 45, 187
[35]. A. Mata, A.J. Fleischman, (2005), S. Roy, Biomed. Microdev. 7, 281
[36]. O. Roure, A. Saez, A. Buguin, R. Austin, P. Chavrier, P. Siberzan, B. Ladoux, (2005), Proc. Natl Acad. Sci. 102, 2390
[37]. F. Schneider, T. Fellner, J. Wilde, U. Wallrabe, (2008),J. Micromech. Microeng. 18, 065008
[38] A.T. Al-Halhouli, I. Kampen, T. Krah, S. Buttgenbach, (2008) J. Microelectr. Eng. 85, 942
[39] J.L. Loubet, J.M. Georges, O. Marchesini, (1984),J. Tribol. 106, 43
[40] M.F. Doerner, W.D. Nix, (1986), J. Mat. Res. 1, 601
[41] B.J. Briscoe, L. Fiori, E. Pelillo, (1998), J. Phys. D Appl. Phys. 31, 2395
[42] S. Roche, S. Pavan, J.L. Loubet, P. Barbeau, B. Magny, (2003), Prog. Org. Coat. 47, 37
[43] J.L. Loubet, W.C. Oliver, B.N. Lucas, (2000), J. Mat. Res. 15, 1195
[44] R. Arinéro, G. L´evˆeque, P. Girard, J.Y. Ferrandis, (2007), Rev. Sci. Instrum. 78, 023703
[45] Y.M. Haddad, (1995), Viscoelasticity of Engineering Materials (Chapman and Hall, London)
[46] D. Tabor, (1951), The hardness of metals (Clarendon Press, Oxford,
[47] C. Cunat, (1996), Rev. Therm. 35, 680
[48] S. Havriliak, S. Negami, (1966), J. Polym. Sci. Part C 14, 99
[49] K.S. Cole, R.H. Cole, (1941), J. Chem. Phys. 9, 341
[50] D.W. Davidson, R.H. Cole, (1950), J. Chem. Phys. 18, 1417